Soft Matter

Adhesion Dynamics of Functionalized Nanocarriers to Endothelial Cells: A Dissipative Particles Dynamics Study

Journal:	*Soft Matter*
Manuscript ID	SM-ART-07-2023-000865.R2
Article Type:	Paper
Date Submitted by the Author:	24-Oct-2023
Complete List of Authors:	Akbari Shandiz, Saeed; Case Western Reserve University, macromolecular science and engineering Khani, Shaghayegh; Case Western Reserve University, Macromolecular Science and Engineering Maia, Joao; Case Western Reserve University, Macromolecular Science and Engineering

SCHOLARONE™
Manuscripts

Adhesion Dynamics of Functionalized Nanocarriers to Endothelial Cells: A Dissipative Particles Dynamics Study

Saeed Akbari (sxa641@case.edu), Shaghayegh Khani (sxk752@case.edu), Joao Maia (jmm272@case.edu)

Department of Macromolecular science and engineering, Case western reserve university

Abstract:

Targeted drug delivery to endothelial cells utilizing functionalized nanocarriers (NCs) is an essential procedure in therapeutic and diagnosis therapies. Using dissipative particle dynamics simulation, NCs have been designed and combined with the endothelial environment, such as the endothelial glycocalyx (EG) layer, receptors, water, and cell wall. Furthermore, the energy landscapes of the functionalized NC with the endothelial cell have been analyzed as a function of properties such as the shape, size, initial orientation, and ligand density of NCs. Our results show that a proper higher ligand density for each particular NC provides more driving forces than barriers for the penetration of the NC. Herein we report the importance of shell entropy loss for NCs shape effect on the adhesion and penetration into the EG layer. Moreover, the rotation of the disc shape NC as a wheel during the penetration is an extra driving force for its further inclusion. By increasing the NCs' size larger than the proper size for each particular ligand density, due to an increase in the NCs' shell entropy loss, barriers surpass driving forces for NC's penetration. Furthermore, the parallel orientation provides the NC with the best penetration capabilities. However, the rotation of the disc shape NCs enhances their diffusion in the perpendicular orientation too. Overall, our findings highlight the crucial role of the shell entropy loss in governing the penetration of NCs. Besides, studying NC with the homogeneous ligand composition enabled us cross barriers and probe energetics after the complete inclusion of the NC.

1. Introduction:

Targeted drug delivery applying functionalized NCs is a critical technique in therapeutic and diagnosis treatments. However, the design of NCs for targeting endothelial cells is still a biomedical and pharmacological challenge.

Successful targeting relies on various physiological factors that control the binding process, including ligand density, the endothelial glycocalyx (EG) layer (composed of carbohydrates like glycoproteins and proteoglycans[1–3]), and receptor expression.[4] The EG layer signifies a thermodynamic impediment to the adhesion of nanoparticles.

In experimental work, Mulivor et al.[5] found that the elimination of the EG layer by enzymatic (heparinase-mediated) degradation significantly affects the adhesion of NCs to endothelial cells. These works emphasize the importance of studying the effects of the EG layer in creating a precise model for nanoparticle adhesion.

Moreover, targeting efficacy is influenced by the number of design parameters such as shape, size, and surface chemistry of NC.[6–12] The latter is defined by the specific interactions between NC surface ligands and the EG chains and cell surface receptors. [13–17]

Researchers[6,8] explored the role of the size and shape of carriers in drug delivery and found that the carrier geometry influences endothelial targeting and disc shape has higher targeting specificity while the sphere diffuses faster into the cell.

Elias et al.[7] developed an experimental strategy to investigate the effect of ligand density of NCs and figured out that cell binding is improved significantly by an intermediate optimal ligand density.

The orientation of NCs at the point where it is attached to the cell defines the local shape of the NCs. Champion et al.[18] discovered that this local shape determines the diffusion rate of NCs into the cell. For instance, an ellipse penetrates very fast through its pointed end while the same ellipse penetrates extremely slower through its flat region.

Computational modeling can be implemented to reduce the time, effort, and cost required for the development of desired NCs,[19–32] by predicting in vivo behavior of NCs and has a considerable impact on biomedical research about NCs delivery to endothelial cells.

There are some models that study the mechanical properties of the EG layer[33,34] and thermodynamic models that investigate the effect of the EG layer on NC binding.[2,35,36]

While simulation studies have played a great role to predict the binding affinities of NCs to endothelial cells, most of the studies so far have investigated the interaction of NCs and endothelium at the continuum level[2,23,36] and haven't provided necessary insight into the molecular structure. A molecular-level simulation is preferred to help us directly track NCs during adhesion and penetration into the EG layer and calculate energetic change for all the physical parameters in the system. [4,37–41]

Cruz-Chu et al.[42] suggested an all-atomistic model for EG chains with all details and high fidelity however due to high computational cost their model cannot be used to investigate large time/scale properties of the EG layer. In a more coarse-grained simulation [2,42–44] the EG layer was studied as a part of the endothelial cell.

Dissipative Particle Dynamics (DPD) is proposed as a mesoscale technique that prevents drawbacks of atomistic and macro scale simulations and is used to explore the dynamics of NCs in the vicinity of vessel wall where environment of endothelial cell will determine the NCs adhesion to targeted areas.[45,46]

Although there have been advances in the understanding of the structure of glycocalyx filaments of endothelial cells and NCs' effect on cellular uptake, NCs' inclusion in endothelial cells has not been sufficiently studied.

Moreover, a systematic study of the individual contributions of design parameters is lacking, leading to a substantial quest for the optimal NC design. Specifically, it is imperative for ligand-functionalized NCs to effectively penetrate the EG chains and access the receptors, enabling ligand-receptor binding.

Using DPD simulation, we suggested a feasible method for incorporating the majority of parameters that control the adhesion process of NCs, including the impact of the EG layer, which, so far, has not been studied with a molecular simulation method.

In this paper, we systemically study the effect of NCs' shape, size, initial orientation, and the effect of NCs' surface chemistry such as ligand density on the adhesion and penetration of NCs to the EG chains and binding of ligands to receptors.

This paper is represented as follows. Section 2 presents the DPD simulation models for functionalized NCs, EG layer, receptor and cell wall, and subsequent methods for examining the penetration of NCs into the EG layer. The potential energy and entropy calculation methods are also explained. In Section 3 we report the influence of the NCs' shape, size, initial orientation, and ligand density on NCs' penetration into the EG layer. The interaction between NCs and EG chains during penetration is calculated through potential energy and entropy analysis. Finally, section 4 concludes our investigation.

2. Methodology

DPD simulation has been proven to serve as a successful method to study soft matters and has accurately captured the physics of functionalized nanoparticles[47–56].

The details of the DPD simulation technique are presented in the supporting information.

In our DPD method, equal bead diameter and equal repulsion parameters for the same components are used[57]. According to Biagi et al.[58], Deng et al.[44] and Neimark et al. [57,59] the particle-particle

interaction parameter is considered equal to solvent-solvent interaction parameters ($a_{SS} = a_{PP}$) and the interaction between different beads (a_{ij}) are chosen as described below. The shell of NCs (labeled N) and ligand with relatively low level of hydrophilicity have the attractive interaction of a_{ij} = 20 with water. Hydrophilic EG and receptor chains have the attractive interaction of a_{ij} = 10 with water. Hydrophilic EG and receptor chains have the attractive interaction of a_{ij} =5 with shell and ligand chains with relatively low level of hydrophilicity. The "core" beads (labeled C) strongly repel all other beads in the system like water, N, and ligand beads with the repulsive interaction of a_{ij} = 40 to ensure that NCs are impenetrable.

The reduced density of DPD beads ρ*=3 and the friction coefficient γ=4.5 are implemented.

According to the original paper of Groot and Warren[60], the number of water beads is adjusted to maintain density of 3 in the system. Water molecules are represented as single beads in this model. The solid wall is made of three parallel layers of fixed beads. The box size is 30×30×60 R_c^3.

In this study, we employ the normalized length, mass, and time scale. The mass of solvent beads is the unit of mass m. The cutoff radius R_c is the unit of length. k_BT is the unit of energy. NVE ensemble is used for DPD simulations with time step $\Delta t = 0.01\tau$ where $\tau = \left(m R_c^2 / k_B T\right)^{\frac{1}{2}}$.

The EG chain is modeled as a bead-spring chain with N=20 segments based on the physics of the EG filament. The harmonic spring constant 100 and the equilibrium bond distance r_{eq}=0.86 are chosen according to the study of Deng et al. [44]. To imitate the molecular structure of actual EG filaments and since the tethered bead of the EG chain is not free to rotate we utilized the EG chains with bush-like structure[38,44]. EG chains are shown in Figure 1.

Table 1 shows the bond information and the interaction parameters for our endothelial system.

In this work, NCs are designed and combined with the endothelial environments such as the EG layer, receptors, water, and cell wall. Simulation results show that we have the ability to prepare features such as the structure and the height of the EG layer and grafting densities of ligands and receptors that follows the experimental observations.

Table 1. Interaction parameters for beads in the system and chain length and bond parameters. The denotation of bead types: N is for the shell of the NC, C is for its core. K is the bond strength and R_e is the equilibrium distance.

Short-range conservative repulsion

aij	EG	receptor	wall	water	C	N	ligand
EG	25.0	25.0	25.0	10.0	30.0	5.0	5.0
receptor		25.0	25.0	10.0	30.0	5.0	5.0
wall			25.0	25.0	30.0	25.0	25.0
water				25.0	40.0	20.0	20.0
C					25.0	40.0	40.0
N						25.0	25.0
ligand							25.0

Chain length and bond parameters

	kT/R_c^2	R_e/R_c		kT/R_c^2	R_e/R_c
EG-EG	100	0.86	EG_wall	100	0.86
NP_NP	500	0.57	ligand_ligand	100	0.57
recep_recep	100	0.86	Ligand_NP	100	0.57
recep_wall	100	0.86			

NC beads are structured into a simple hexagonal lattice bonded through harmonic bonds. We keep the equivalent surface area for different NC shapes instead of the surface area to volume ratio, first because the surface area defines the capacity of the NC to load it with the drug.

Second, at a specific ligand density, it is required to have the same number of ligands on every shape of the NCs.[45,61,62] Thus, different shapes of NCs can exhibit equal binding strength between ligands and receptors, helping us explicitly analyze the impact of the shape on the adhesion of NCs to the endothelial cell. According to grafting density, ligand beads are permanently grafted at random beads on the NC outer layer.

Three NC diameters, 8 R_c, 12 R_c, and 16 R_c are made. These three sizes are constructed for the disc and rod shape of the NC with equal surface areas to the sphere. Functionalized NCs for sphere, disc, and rod shapes are shown in Figure 1.

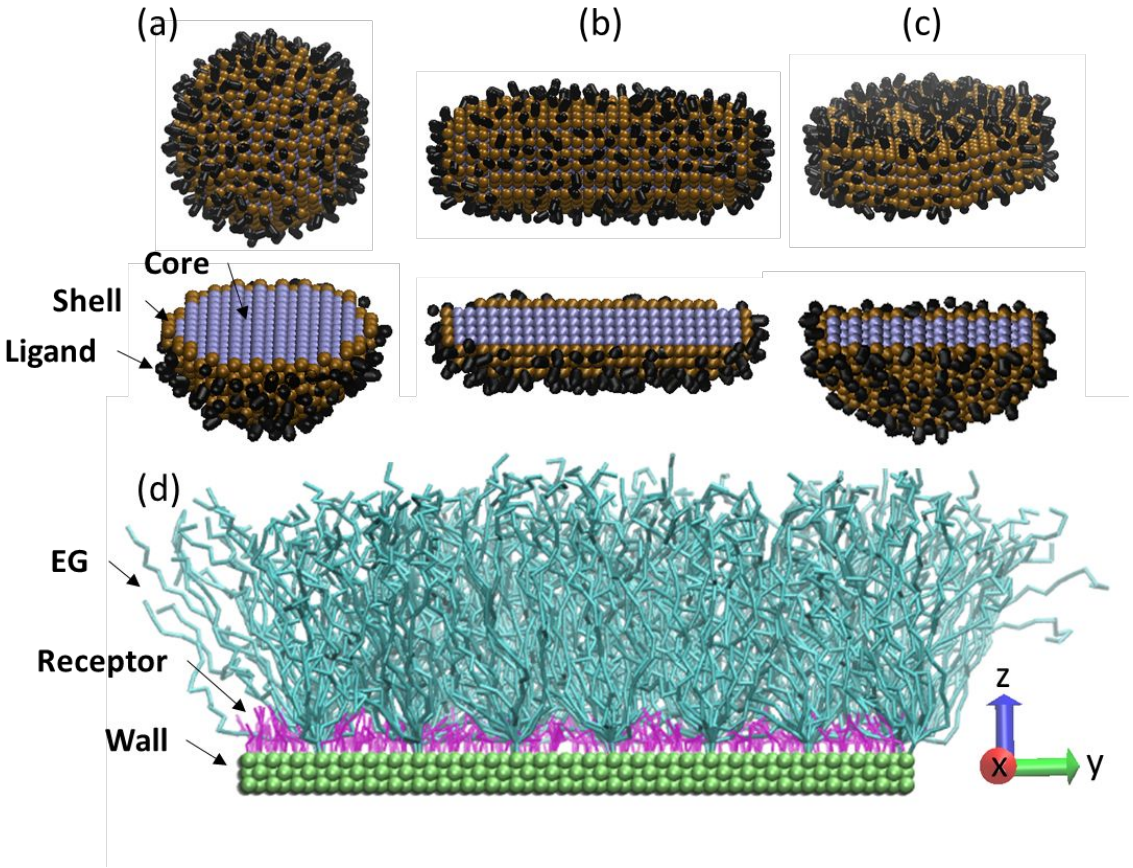

Figure 1. Model of (a) spherical shape, (b) rod shape, (c) disc shape of functionalized NCs with hydrophilic ligands (black), shell layer (brown) and core (blue), and (d) EG chains (blue), receptors (pink) and cell wall (green). The size of the NC is 12 R_c.

DPD simulations are conducted for $10*10^5$ time steps until the system reaches the equilibrium state. To determine the time taken for the system to reach equilibrium, we monitor the temperature of the entire system until it stabilized at 1. After 10*10^5 time steps, we observe no fluctuations in temperature, indicating that the system has reached the intended equilibrium state[60].

During the equilibration of the system, the NC is in the bulk water. Then the NC is located on top of the EG layer and another $30*10^5$ time steps of NVE simulation is performed to study the

adhesion and penetration of the NC to the EG layer. In fact, this $30*10^5$ time steps run is enough to study the complete penetration of the NCs through the EG layer and reach the receptor area. In this study, three independent runs are conducted for the DPD simulation of each sample, and the average of these three runs is plotted for all the properties.

In order to interpret the reason for the adhesion or repulsion of NCs by the endothelial cell we need to monitor the variation of free energy contributions to this process.

We have studied the free energy of adhesion and penetration, which includes potential energy and entropy terms.
In most energy studies of NPs adhesion to polymer brushes, energy is calculated related to the NP distance from the substrate inside the polymer brush. However, in our dynamic study, the adhesion and penetration of NCs to the EG layer can be visualized and at the same time, the energy change can be recorded. So, this method helps us discover and interpret previously unseen events like the rotation of NCs during the penetration into the EG layer.

The detail of the potential energy and entropy calculation is explained in the supporting information.

In recent works, conformational entropy has been calculated as a main fingerprint to quantify deformations and changes in the conformation of soft materials[63–65]. We measure conformational entropy as well, to identify conformational deformations in the environment of endothelial cells.

The entropy is always negative, and the lower entropy demonstrates the more ordered environment. In general, penetration of NC to the EG layer occurred when the driving force is larger than the barrier.

3. Results and discussion:

In this section, we study the influence of a series of factors on the functionalized NCs adhesion and penetration into the EG layer. First, we analyze the shape effect. Second, we use NCs with the best shape to study the effect of size. Third, we use NCs with the best size to investigate the effect

of the NC's initial orientation to find the best position of the NC on top of the EG layer. Finally, the best orientation is used to evaluate the effect of ligand density. The interaction between NCs, EG and receptor chains during the penetration is quantified through potential energy and entropy calculations.

3.1. Shape effect:

One of the parameters that affect the targeting capability of NCs is their shape. In fact, both the surface area available for targeting ligands and the local curvature of different shapes of NCs influence the ligand adsorption and the amount that NCs fit the contours of the cell.[66]

On the other hand, NCs with different biological applications require different shapes which have been investigated extensively.[67–70] For instance, in a simulation study, the anisotropic NCs are adsorbed into the polymer brushes more difficult than spherical NCs.[71]

Accordingly, in our study, it is essential to understand how the shape of NCs can control their penetration in the EG layer and their adhesion to receptors of the cell. In figure 2, snapshots, density profiles, potential energies, and entropies of the 12 R_c functionalized NCs are plotted as a function of shape. In figure 3, Rg_Z plots of the EG chains are shown as a function of shape, size, initial orientation, and ligand density of NCs.

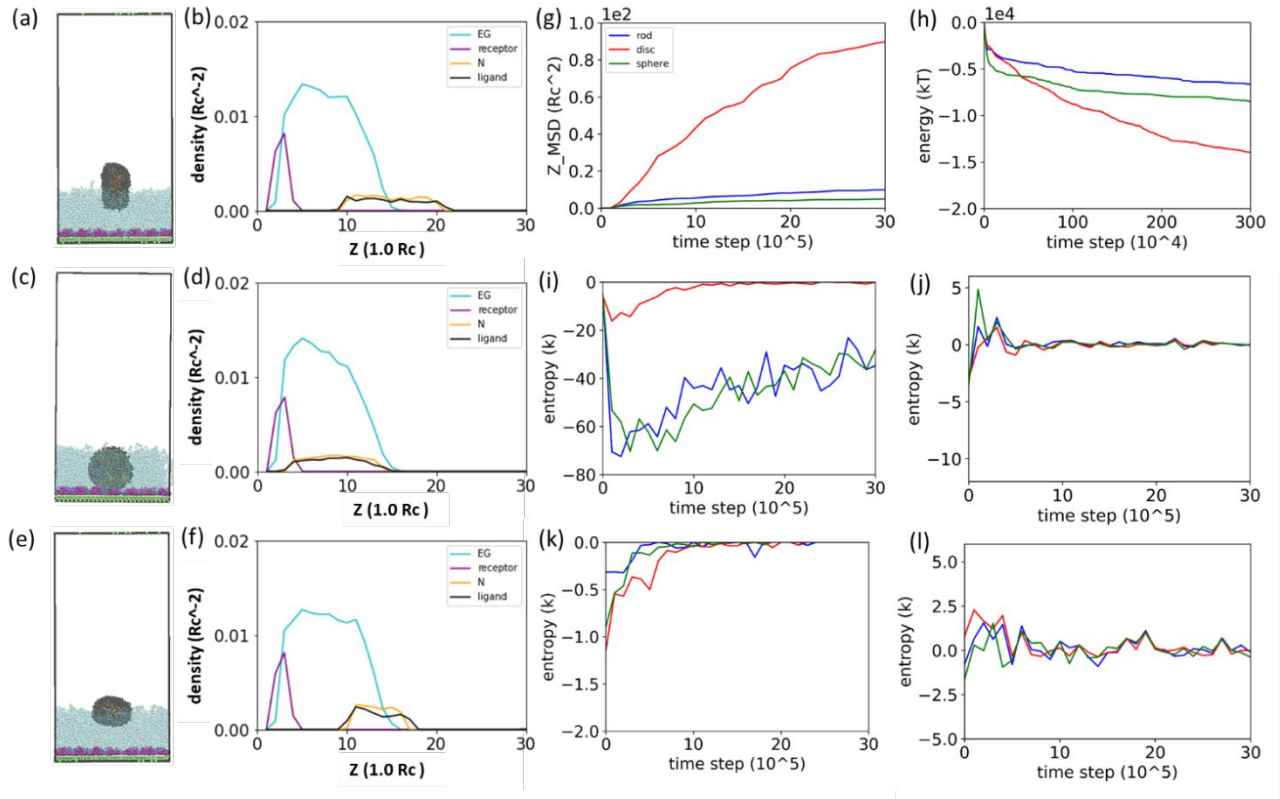

Figure 2. VMD snapshot and density profile of (a), (b) rod, (c), (d) disc, and (e), (f) sphere after $30*10^5$ time steps run. The time evolution of (g) Z_MSD, (h) potential energy, (i) shell entropy, (j) EG entropy, (k) ligand entropy, and (l) receptor entropy of 12 R_c NCs with different shapes. The red curves indicate disc shape NC, while blue and green indicate rod and sphere shape NCs, respectively.

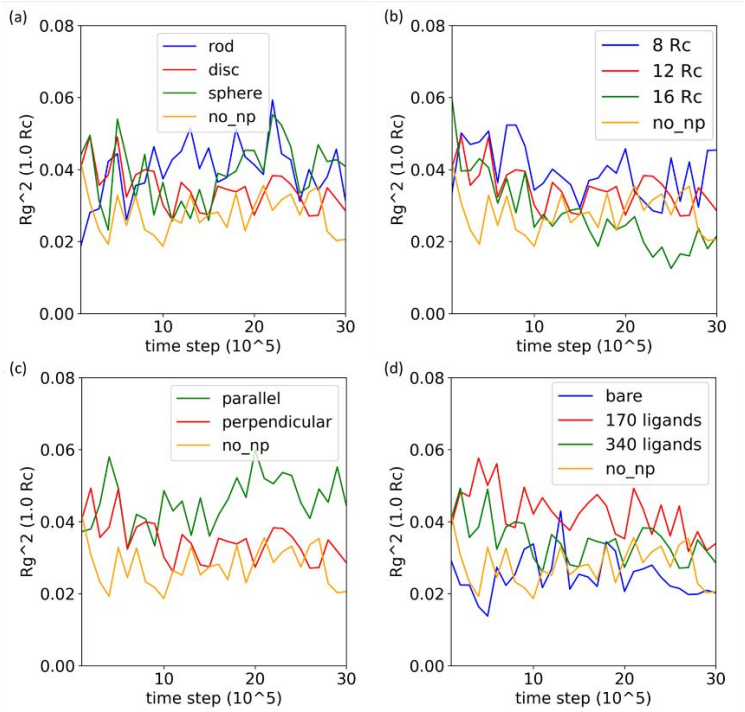

Figure 3. The time evolution of Rg^2 in Z axis for the EG chains as a function of (a) shape, (b) size, (c) initial orientation, and (d) ligand density of NCs. Yellow curves show the Rg^2 in Z axis of unembedded EG chains (no_np).

Density profiles (Figures 2a-2b, 2c-2d, 2e-2f, and S3a-S3b, S3c-S3d, S3e-3f) show that during the simulation, the shell size (N) increases for the rod and sphere shapes, indicating significant entropy loss in the shell. In contrast, for the disc, shell and ligand densities are similar and distributed smoothly. This efficient ligand coverage allows the disc to rotate freely among the EG chains. However, in the case of the rod and sphere, there is a disparity between ligand and shell density, leading to uneven ligand distribution on the shell. Consequently, the rod and sphere shapes cannot rotate and penetrate as effectively as the disc. (Figure 2g).

The NC adhesion and penetration to the EG layer and cell surface are mainly determined by the delicate balance between the energetic gain due to the ligand-EG and ligand-receptor binding and the entropies of various components including EG, NC's shell, ligands, and receptors.[37]

At the initial steps of simulation, NCs with identical surface area, interaction strength, and grafting density of the ligands, but with different shapes show different potential energies for the penetration (Figure 2h). The explanation lies in the work of Ding et al.[72] who demonstrated that

the local shape (surface area) of the NC on the EG layer determines the initial potential energy. Because the sphere has more surface area in contact with EG compared to the rod and the disc, it possesses the highest driving force. The minimum energy observed at the ligand-receptor area signifies that, in the case of the disc with complete penetration, ligands bind to receptors, leading to the lowest potential energy for the disc.

However, the rod and the sphere struggle to penetrate effectively, resulting in a consistent trend of potential energy from beginning to end. Despite the initially higher potential energy for the sphere, penetration efficiency is not solely determined by potential energy; it is influenced by the entropy losses induced by the NCs' penetration.

It should be noted that the difference between penetration amounts of different NC shapes is governed by either the difference between potential energies of these shapes or the difference between their entropy losses. In other words, when it is mentioned that for the shape effect, the penetration amount is controlled by NCs entropy it means that the trend of penetration amount is consistent with the trend of NCs entropy and not with the trend of potential energy.

The shell entropy plot shows a significant increase in entropy loss for the rod and the sphere compared to the disc (Figure 2i). To explain this behavior precisely, we investigated the shape effect on two other groups of samples. In the first group, there are 12 R_c bare NCs with different shapes and in the second group, 8 R_c ligand functionalized NCs with different shapes are studied. As it is shown in figure S1, for 12 R_c bare, the shell entropy of the rod (around -100 K) is larger than the shell entropy loss of 12 R_c ligand functionalized rod (around -80 K). This indicates that the presence of ligands dissipates the force on the NC shell and so decreases the shell entropy loss for all different shapes.

Gao et al.[71] discovered that when the nanoparticle is at the interface of the polymer brush and the solvent, the surface tension controls the inclusion free energy. However, when the nanoparticle has a deep inclusion inside the polymer brush the osmotic pressure determines the free energy changes.

Accordingly, for 8 R_c ligand functionalized NCs (figure S2) it is seen that the sphere has a significantly larger shell entropy loss than the rod and the disc. In fact, when the rod and the disc

are adsorbed by EG chains they can penetrate inside with their slim edge in contact with the EG layer, hence they feel lower surface tension than the sphere with a wide local area and so they have lower shell entropy loss.

However, for 12 R_c bare NCs (figure S1), it is observed that like the 12 R_c ligand functionalized NCs (figure 2), sphere and rod have a huge increase in shell entropy compared to disc. In fact, at this size, the surface area of the rod in contact with the EG layer is as wide as the sphere's surface area so both the rod and the sphere feel a large surface tension and have high shell entropy losses.

Over time, the shell entropy loss of the disc diminishes, while the rod and sphere continue to experience high shell entropy losses. To understand this, examining the behavior of 12 R_c bare NCs is instructive. Since there's no penetration inside the EG chains, the shell entropy for the sphere and rod remains significantly higher than that of the disc, persisting until the end of the simulation. In contrast, for the 8 R_c ligand functionalized sphere and disc capable of penetration (Figure S2), the shell entropy loss fluctuates around zero. One possible explanation is that when the sphere or the rod is inside the EG layer, the NC feels the osmotic pressure of EG chains which is applied to the volume of the NC so causes low entropy loss of the shell. However, when they cannot penetrate inside the EG layer like the bare sphere and bare rod, the NC feels the whole surface tension of the EG layer only on its edge's surface area which leads to a large entropy loss of the NC. Therefore, the osmotic pressure can cause less shell entropy loss for NCs than the surface tension.

In a theoretical study and a DPD simulation [73,74] of an elastic NC interacting with a cell membrane, it is revealed that for soft NCs it is more difficult to penetrate into the membrane than for rigid NCs and this is due to the existence of the extra bending energy of the NC itself.

Moreover, our observation indicates that since NCs with similar flexibilities (softness) do not want to lose the freedom of motion of their shell beads therefore only NCs can penetrate that can keep their disordered shell. For this reason, they need to have a slim edge like a disc in contact with the EG layer.

Figure 2j depicts that the sphere has a lower entropy loss of EG chains. As it is shown in Figure S9, for all NC shapes, EG chains are more disordered than the the unembedded EG chains. In fact,

the functionalized NC with its high attractive interaction with the EG layer can provide the EG chains more freedom to move. Therefore comaring the rod and the disc, the sphere with a higher attractive interaction with the EG layer can make the EG layer more disordered. Overall, EG entropy is a strong deriving force for the sphere's pentertaion.

The time evolution of Rg for EG chains in Figure 3a demonstrates that all shapes can expand EG chains more than unembedded EG chains. Moreover, with more penetration of NCs, Rg of EG chains decreases more toward the Rg of unembedded EG chains. Moreover, rod expands the Rg of EG chains more than other shapes. Comparing the EG entropy and the Rg of EG chains for different shapes, it can be deduced that the increase in Rg of EG chains triggered by the NCs penetration makes EG chains more disordered.

For the ligand entropy over time (Figure 2k), a similar trend to the shell entropy can be observed. The ligand entropy loss decreases with the NC's penetration to the EG layer. The disc shows a higher amount and longer time of the ligand entropy loss than the other shapes due to its higher depth and longer time of penetration. For the disc, the entropy loss of ligand over time (Figure 2k) is significantly high. Indeed due to the lower attractive interactions of ligands with EG chains, ligand chains of the disc are more ordered.

However, for the rod and the sphere their higher attractive interaction with the EG layer provides ligand chains with more freedom to move. Therefore, at these shapes, the NC has more disordered ligand chains.

As it was mentioned above, comparing to the disc, for the rod with a higher attractive interaction with the EG layer, the EG chains are also more disordered. It can be concluded that the attractive interaction between EG and ligand chains makes both the EG chains and ligand chains more disordered. Comparing to other shapes, ligand entropy is a nominal barrier for the pentertaion of the rod shape NCs.

Figures 2l and S13 show that there is not a clear distinction between the receptor entropy losses. But it is expected that the penetration of the disc, which leads to denser and more ordered EG chains, resulting in more ordered receptors.

Kumar Sadhu et al[75]. Champion et. al[18] and G. Sharma et al[76] studied engulfment of NCs with different shapes. They observed that when the shape deviates from a sphere the engulfment times increase. In our study the shell deformation of NCs with various shapes provides them different capabilities. In fact, although the disc has the lower driving force like potential energy and higher barriers such as the entropy loss of ligands, the sphere and the rod have a significantly higher shell entropy loss than the disc. Therefore, the disc can penetrate better. In summary, at different shapes, shell entropy loss controls the penetration.

Finally, according to Wang et.al[78] and Walker et.al[79], studying various shapes allows for the manipulation of molecular environments within ligands, leading to distinct surface chemistries.

Consequently, molecules positioned on surfaces with varying curvatures can display diverse interactions and penetration depths despite being the same molecule.

3.2. Size effect:

To characterize how the size of NCs can affect their penetration in the EG layer snapshots, density profiles, potential energys, and entropies of the system as a function of NC diameter are plotted in figure 4.

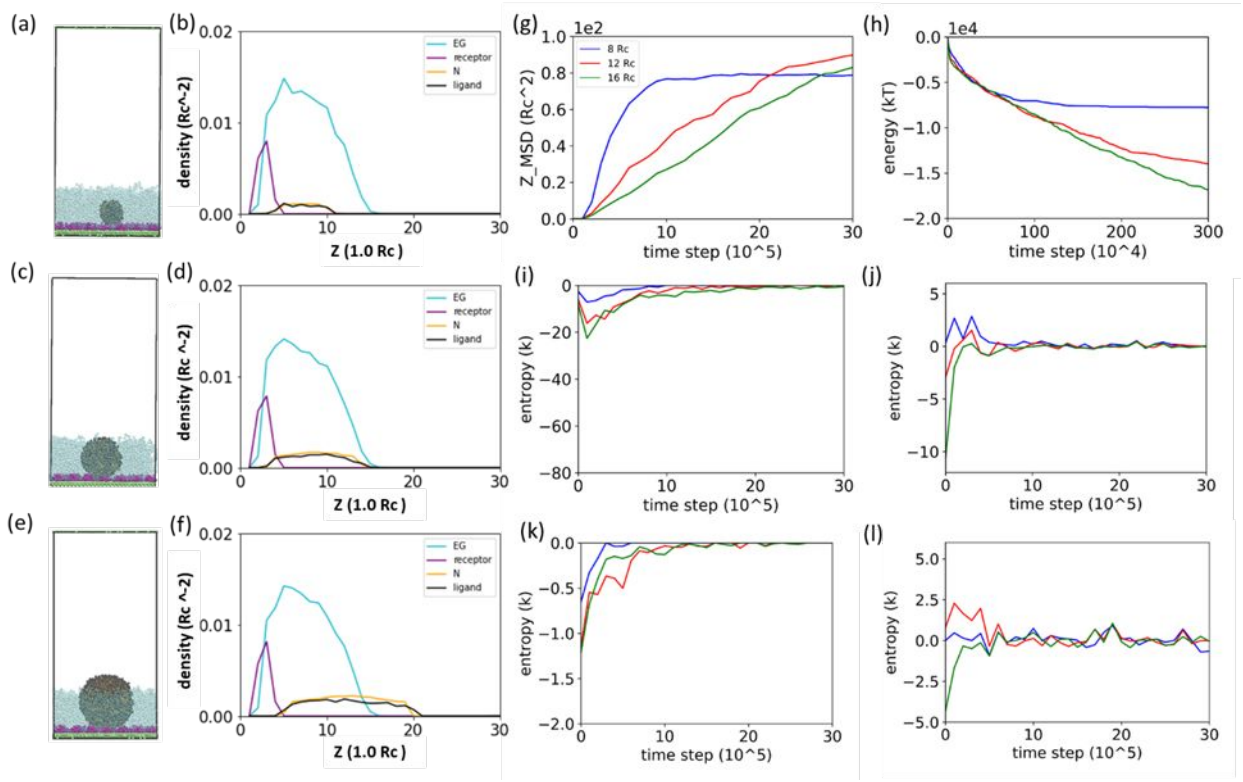

Figure 4. VMD snapshot and density profile of (a), (b) 8 R_c, (c), (d) 12 R_c, and (e), (f) 16 R_c disc after 30*10^5 time steps run. The time evolution of (g) Z_MSD, (h) potential energy, (i) shell entropy, (j) EG entropy, (k) ligand entropy, and (l) receptor entropy of discs with different sizes. The blue curves indicate 8 R_c NC, while red and green indicate 12 R_c and 16 R_c NCs, respectively.

Density profiles shown in Figures 4a-4b, 4c-4d, and 4e-4f illustrate that diameters of our NCs are exactly 8 R_c, 12 R_c, and 16 R_c. Moreover, it is seen that by increasing the size of the disc from the 8 R_c (a smaller size than the EG height) to the 16 R_c (a larger size than EG height), the penetration speed decreased significantly (Figure 4g). The density profiles indicate that larger NCs require more time for EG chains to cover all the ligands on the NC. However, a notable observation is that the very large disc (16 R_c) can penetrate the EG layer with a height shorter than its diameter. Figure S4 illustrates that the 16 $R_c$disc, after staying at the EG-water interface for some time, begins rotating backward and forward around 7*10^5 time steps. Through this rotation, the disc initiates a diffusive motion. This is a unique feature of the disc NC and has not been observed for other shapes of NCs. Furthermore, it is seen that for these three sizes, the ligand density is like the shell

density. Thus, as mentioned above, this unique behavior provides the three sizes of the disc with the capability of rotation and complete penetration inside the EG layer (figures S6 and S7).

The amount of potential energy (Figure 4h) at the initial steps implies that all different sizes of the NC with the same ligand density have the same initial potential energy. Wang et.al[78] and Walker et.al[79] noted that as the NP size increases, its curvature decreases, leading to a reduced average distance between ligands and consequently a lower fraction of ligands. Despite larger NPs having more ligands, our study found that the increase in NP size was balanced by the decrease in ligand surface density, resulting in similar potential energy between larger NPs and smaller NPs.

Minimum energy at ligand-receptor area shows that the 16 R_c has the largest exhausting of ligands by binding of ligand-receptors and has the lowest potential energy. Although all different sizes have the same initial driving force, the penetration speed does not follow the potential energy trend and therefore is determined by the amount of entropy losses of the penetration. In fact, for the 12 R_c NC, the employed ligand density generates enough driving forces to overcome barriers caused by its large size but for 16 R_c NC driving forces are not enough to defeat barriers of such a large size NC as well. This implies that the penetration is determined by the amount of entropy losses.

Investigating entropies, it is observed that the 16 R_c disc has the largest shell entropy loss (Figure 4i) and EG entropy loss (Figure 4j).

Gao et.al [71] explored the effect of size on the inclusion energy of NC in a polymer brush. They showed that for a polymer brush with a high grafting density, like the grafting density of EG chains in our work, with nanoparticles at the polymer/solvent interface, penetration free energy is affected by surface tension of the form $\sim R_{NP}^2$. However, when nanoparticles have a deep penetration inside the polymer brush, penetration free energy is influenced by osmotic pressure of the form$\sim R_{NP}^3$.

Thus, the larger is the NC the more difficult is the penetration of NC into the EG layer, and this difficulty is reflected in the EG entropy and the shell entropy losses. Furthermore, the contact area between the NC and the cell surface defines the penetration capability of NCs.[72]As it was mentioned before since the local surface area of the larger disc is wider than smaller discs so initially, it feels more surface tension and therefore has more shell entropy loss. It also indicates

that the smaller disc has more mechanical stiffness than the larger one, so the smaller disc has less shell entropy loss.

Over time, the NC shell entropy loss decreases with more penetration of the NC and when the 8 R_c disc is completely inside the EG layer the shell entropy loss is zero. One possible explanation is that osmotic pressure deforms the shell only during the penetration so when the NC reaches to the receptor area and its ligands are bonded to the receptors the osmotic pressure does not deform the NC's shell anymore.

As it is illustrated in Figure 4j, 8 R_c disc shows a lower entropy loss of EG chains and thus 8 R_c disc makes EG chains more disordered. Furthermore, as it is shown in Figure S10, with the penetration of all sizes of the disc, EG chains get more disordered than unembedded EG chains. In fact, all sizes of NCs with the attractive interaction with the EG layer can provide EG chains more freedom to move.

Although larger size NCs have more attractive interaction with EG chains, the penetration of larger size NCs leads to more ordered EG chains than the penetration of smaller size NCs. The reason for this behavior is that, larger NCs occupy more space between EG chains and so EG chains have less freedom of motions. In other words, EG entropy follows the trend of shell entropy and since the local surface area of a larger disc is wider than smaller discs, initially it causes more EG entropy loss. Besides, the penetration of larger NCs with a more ordered shell, resulted in more ordered EG chains. Hence, there is a direct relationship between the ordering of EG chains and the NC's shell.

Overall, for large NC sizes in addition to the attraction of EG chains and ligands, the size induced restriction on the conformation of EG chains controls the EG entropy. Moreover, EG entropy is a strong deriving force for the pentertaion of the smaller disc.

The time evolution of Rg of the EG chains in Figure 3b demonstrates that the penetration of all sizes of NCs can expand EG chains more than unembedded EG chains. Moreover, with more penetration of NCs, Rg of EG chains decreases more toward the Rg of unembedded EG chains. Only the 16 R_c disc penetration occupies a large space among EG chains and therefore the Rg of EG chains reduces less than that of unembedded EG chains. Moreover, 8 R_c disc expands the Rg

of EG chains more than other sizes due to the less restriction on the conformation of EG chains. Comparing the EG entropy and the Rg of EG chains for different sizes of NCs, it can be concluded that the increase in the Rg of EG chains due to the NCs penetration makes EG chains more disordered.

The entropy change of ligand over time (Figure 4k) is larger for the 12 R_c than the 16 R_c NC and therefore its ligand chains are more ordered. This behavior aligns with our expectations that the larger NC with the lower potential energy produces more disorderd EG chains and more disorderd ligand chains. Though the 8 R_c NC shows more disordered ligand chains than larger NCs. To explain the reason, as it is mentioned for the EG entropy, larger NCs occupy more space in between EG chains and make them more orderd. However, the 8 R_c disc with a smaller diameter than the EG layer height does not occupy that much a space. It was seen before that there is a direct relationship between the ordering of EG chains and ligand chains. For the size effect also, ordering of EG chains with the penetration of larger NCs makes ligand chains more ordered. Comparing to larger size discs, the ligand entropy is a weak barrier for the pentertaion of smaller size discs.

Although all NC sizes can completely penetrate inside the EG layer and reach to the receptor layer and have ligand/receptor binding, the entropy loss of receptors is lower for 12 R_c disc (Figures 4l, S14). The reason is that comparing to 8 R_c NC the12 R_c NC with a higher attractive interaction can penetrate more and get closer to receptor chains and make them more disorderd. For 8 R_c the receptor entropy is not significantly different than unembedded receptor entropy. Comparing to 16rc, 12 R_c has more disordered EG chains causes more disordered receptor chains.

Kumar Sadhu et al.[75] investigated the engulfment of nanoparticles (NCs) of different sizes. They discovered that extremely small particles cannot be internalized due to high bending energy, while excessively large particles require larger vesicles for complete internalization.

In our work, although larger NCs have more driving force for the penetration such as a low potential energy, their barriers such as shell and ligand entropy losses are higher, thus they have slower dynamics. On the other hand, NCs smaller than a certain threshold exhibits a low driving force for the penetration. Therefore, NCs with the moderate size (12 R_c) possess sufficient deriving force to overcome barriers, enabling faster and more effective penetration.

3.3. Orientation effect:

The penetration of a NC into the EG layer is directly related to the initial orientation of the NC, $\emptyset_0$ (Figure S8). In fact, the orientation of NCs at the point where it is attached to the cell defines the local shape of the NCs. Champion et al.[18] discovered that this local shape determines the diffusion rate of NCs in the cell. In a DPD simulation study by Yang et al.[77], it is observed that the initial orientation of a nanoparticle affects its interaction with the cell membrane substantially.

Therefore, it is crucial to understand the effect of NCs orientation on their adhesion and penetration into the EG layer. For this purpose, snapshots, density profiles, potential energies, and the entropies of the system as a function of NC orientation are plotted in figure 5.

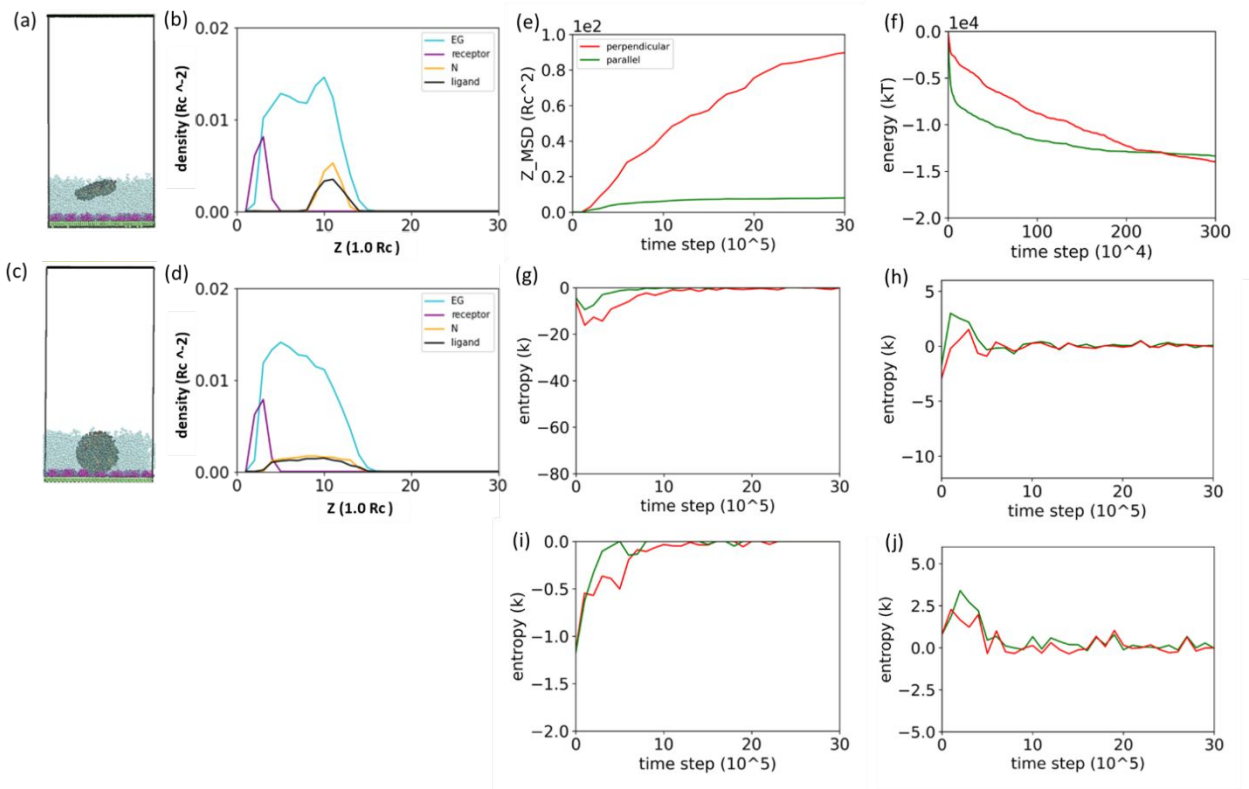

Figure 5. VMD snapshot and density profile of (a), (b) parallel, and (c), (d) perpendicular orientation of 12 R_c disc after $30*10^5$ time steps run. The time evolution of (e) Z_MSD, (f) potential

energy, (g) shell entropy, (h) EG entropy, (i) ligand entropy, and (j) receptor entropy of 12 R_c NCs with different initial orientations. The red curves indicate perpendicular orientation, while green indicate parallel orientation.

The density profiles (Figures 5b, and 5d) show that the parallel-oriented disc exhibits lower ligand density than shell density, limiting deep penetration in the EG layer. Conversely, perpendicular-oriented discs, with equal ligand and shell density, rotate freely within EG chains, enabling deeper penetration.

In fact, according to Wang et.al[78] and Walker et.al[79] the greater the curvature of NCs, the greater the average distance between ligands. In simpler terms, changes in the curvature across the particle's surface led to variations in ligand surface density. Therefore, the parallel-oriented disc with the higher curvature at the edge has a lower surface density of ligands. Consequently, this orientation of disc yields the lower contact of the ligands with the perpendicular-oriented EG chains.

Conversely the perpendicular-oriented disc with two flat surfaces has higher surface density of ligands which enhances the contact of the ligands with the perpendicular-oriented EG chains.

Furthermore, this presence of the disc with parallel orientation among the EG chains results in the increase of the EG chains density around the disc.

The amount of driving force (Figure 5f) at the initial steps reveals that while both NCs with 0° (perpendicular) and 90° (parallel) orientations have the same ligand density, parallel has more ligands in contact with the EG layer so has a lower potential energy or a higher driving force. Minimum energy at the ligand-receptor area indicates that both the parallel and perpendicular orientations can completely go inside the EG layer and have a large exhaustion of ligands through the adhesion of ligand-EG. Though the driving force is initially higher for the parallel orientation its penetration is significantly slower than the perpendicular orientation which implies that the penetration is determined by the amount of entropy losses.

Exploring the entropies, reveals that perpendicular orientation initially has a larger shell entropy loss (Figure 5g). The parallel-oriented disc demonstrates greater mechanical stiffness against the surface tension at the EG/water interface.

As it is illustrated in figure S5, for the 8 R_c rod also the parallel orientation has the lower shell entropy loss than the perpendicular orientation. Moreover, during the penetration of the disc into the EG layer, the entropy loss of the shell decreases due to osmotic pressure of EG chains until the parallel disc stops moving among the EG chains or ligands of perpendicular disc bind to the receptors.

EG entropy plot (Figure 5h) shows that the penetration of the parallel orientation, with a higher attraction of EG chains and ligand, offers a lower EG entropy or more disordered EG chains than the penetration of the perpendicular orientation. As it is shown in Figure S11, by penetration of the disc with these orientations, EG chains are more disordered than the unembedded EG chain. In fact, by having the attractive interaction between ligands and EG chains, these orientations of NCs can provide EG chains with more freedom to move.

Besides, the penetration of the parallel orientation with a more disordered shell, resulted in more disordered EG chains. In summary, the EG entropy is a strong deriving force for the pentertaion of parallel orientations of NCs.

The density profile of the parallel orientation (Figure 5b) shows that the penetration induces an increase in the density of EG chains around the EG/water interface. The density profile of perpendicular orientation (Figure 5d, S3f and S3g) displays that the penetration leads to an increase in the density of EG around the receptor area. These local increases in the density of the EG layer results in a higher expansion of EG chains than EG chains without NCs.

The time evolution of the Rg of EG chains in Figure 3c clearly illustrates that parallel and perpendicular orientations of the disc can expand EG chains more than the unembedded EG chains. Moreover, with more penetration of NCs, the Rg of EG chains decreases more toward the Rg of the unembedded EG chains. Moreover, the parallel orientation of the disc, with its higher density at the interfacial area, increases the density of EG chains and therefore expands the Rg of EG chains more than the perpendicular orientation. Comparing the EG entropy and the Rg of EG

chains for different ligand densities, it can be deduced that the increase in the Rg of EG chains by the NCs penetration makes EG chains more disordered.

Moreover, for the parallel orientation the ligand entropy loss (Figure 5i) is lower. For this orientation, ligand chains have a very attractive interaction with the EG layer and and the Rg of EG chains is increased. Therefore, parallel orientations of NCs can provide ligand chains with more freedom to move. As it was mentioned above, for the parallel orientation the EG chains are also disordered. Thus the attractive interaction between EG chains and ligands makes both EG chains and ligands more disordered. Comparing to the perpendicular orientation, ligand entropy is a weak barrier for pentertaion of the parallel orientation.

Although, the perpendicular orientation of the disc can completely penetrate inside the EG layer and have ligand/receptor binding, the entropy loss of receptors is higher for the perpendicular orientation than the parallel one (Figures 5j, S15). Density profiles show that for the parallel orientation more stretched part of EG chains are near the receptor layer but for the perpendicular orientation the denser (collapsed) part of EG chains is near receptors. Therefore, more stretched part of EG (more disordered EG chains) causes more disordered receptor chains.

According to Kumar Sadhu et al.[75] oblate NCs with the top close to the vesicle can be engulfed slower than oblate NCs with the side in contact with the vesicle. In our work also, it is expected that the disc in the perpendicular orientation (the top in contact with the EG layer), with lower driving forces such as the potential energy, EG chains and receptors entropy losses and higher barriers such as entropy losses of the shell and ligands, has slower dynamics than the parallel orientation. Though, as mentioned before the perpendicular orientation of the disc can rotate clockwise and counterclockwise and this capability has a stronger effect on the penetration than the entropy losses of ligands or the shell. Hence the perpendicular orientation of the disc can penetrate better than the parallel orientation. In figure S7, the VMD snapshots for the rotation of the perpendicular disc at different time steps are shown. This 12 R_c disc shows a higher MSD value which indicates that besides the penetration inside EG chains in the Z-direction the disc can rotate and move forward in the X-direction. As it is illustrated in figures S6 and S7, the 8 R_c disc can rotate more and therefore can penetrate faster than the 12 R_c disc.

In general, there are different final penetration depths and energies for these NCs. It implies that the final states of NCs clearly depend on their initial orientation. Actually, the orientation of NCs at the EG/water interface defines the local shape of NCs and the diffusion rate in the cell is determined by those local shapes[18]. In other words, initial driving forces for NCs penetration to the EG layer greatly vary by the initial contact area of NCs with the EG layer and the final penetration depths and energies of NCs are determined by these initial orientations.

3.4. Ligand density effect:

To assess the effect of ligand density of functionalized NCs on the interaction of NCs with the EG layer and receptors, we calculate the potential energy and entropy of the penetration of NCs without ligands, with low and high ligand densities into the EG layer. Figure 6 shows snapshots, density profiles, potential energies, and the entropies of the system as a function of NC ligand density.

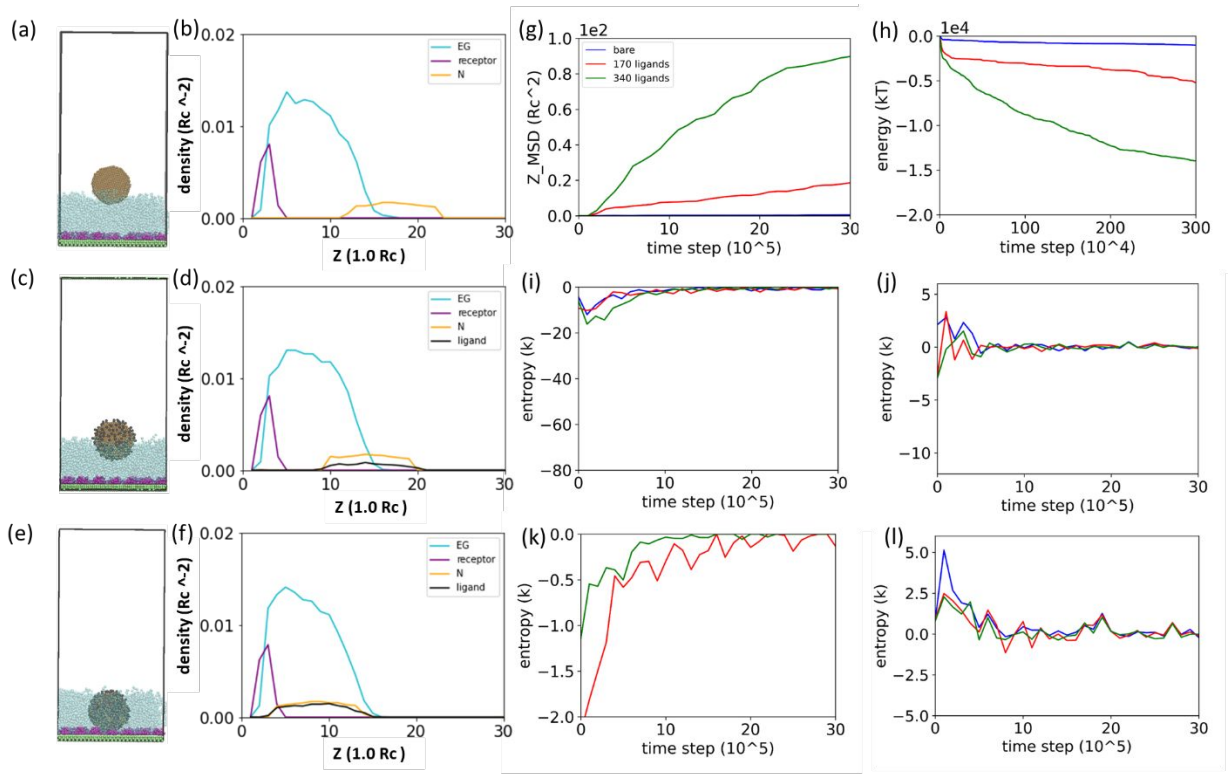

Figure 6. VMD snapshot and density profile of (a), (b) bare, (c), (d) 170 ligands, and (e), (f) 340 ligands after $30*10^5$ time steps run. The time evolution of (g) Z_MSD, (h) potential energy, (i) shell entropy, (j) EG entropy, (k) ligand entropy, and (l) receptor entropy of 12 R_c discs with different ligand densities. The blue curves indicate bare NC, while red and green indicate NC with 170 ligands and 340 ligands, respectively.

The density profiles (Figures 6a-6b, 6c-6d, and 6e-6f) show that in the bare disc, there is an expansion of EG due to the EG chains covering the surface of the shell instead of binding to the ligands, as observed in ligand-functionalized discs. As mentioned earlier, in discs with high ligand density where ligands cover the shell, complete penetration is possible, allowing the disc to rotate and penetrate fully (Figure 6g). The optimal ligand density is achieved when ligands and shell densities at the EG/water interface match. Additionally, the density profiles demonstrate that in discs with 340 ligands, complete penetration increases the density of EG chains in the area close to receptors.

The amount of the potential energy (Figure 6h) at initial steps implies that the NC with higher ligand density has a lower potential energy or a larger driving force. The presence of ligands enhances the driving force significantly for low and high ligand densities more than the bare NC. Minimum energy at the ligand-receptor area suggests that the NC with higher ligand density which penetrates more has the largest exhausting of ligands through the adhesion of ligand/EG and ligand/receptor. Since the trend of penetration is like the trend of the potential energy, thus, the potential energy difference determines the penetration amount.

On the other hand, the amount of entropy for the penetration in Figure 6i shows that the 340 ligands disc initially has a larger shell entropy loss than the 170 ligands and the bare disc which is due to the surface tension force triggered by the EG layer. As it was explained about the dominant role of potential energy on the penetration, the high ligand density NC with the lowest potential energy has the fastest penetration into the EG layer. This fast initial motion leads to a high surface tension at EG/water interface and thus high shell entropy loss for the disc.

Over time the entropy loss of the shell, which is influenced by the osmotic pressure of the EG layer, decreases by the penetration of NCs inside the EG layer and when the 340 ligands disc is completely inside the EG layer it reaches zero. Besides, since the 170 ligands disc has a shallow penetration inside the EG layer, it has larger entropy loss of the shell than the bare disc due to the surface tension of the EG layer.

Figure 6j displays that for the NC with 170 ligands the EG entropy is lower and hence EG chains are more disordered than for the NC with 340 ligands.

Despite the stronger attractive interaction between the NC with 340 ligands and EG chains, its faster penetration results in more ordered EG chains compared to the penetration of the NC with 170 ligands. This phenomenon occurs because the extensive penetration of the NC with 340 ligands occupies more space between EG chains, limiting the freedom of motion for the EG chains.

On the other hand, as it is shown in Figure S12, for low and high ligand density NCs, EG chains are more disordered than unembedded EG chains. In fact, by having more attractive interaction between ligands and with EG chains, ligand functionalized NCs can provide EG chains more freedom to move. Only the penetration of the bare NC with the lowest attractive interaction with

the EG layer make EG chains as ordered as EG chains without NCs. Comparing to the high ligand density NC, EG entropy is a strong deriving force for the penetration of the low ligand density NC.

Comparing the EG entropy and the Rg of EG chains (Figure 3d) for different ligand densities, it can be deduced that NCs penetration increases the Rg of EG chains and makes them more disordered than unembedded EG chains.

The time evolution of Rg of EG chains displays that high and low ligand density discs can expand EG chains more than unembedded EG chains. However, with the more penetration of the high ligand density NC, Rg of EG chains decreases toward the Rg of unembedded EG chains. Only the bare disc penetration with the lowest attractive interaction with the EG layer does not expand the Rg of EG chains more than that of the unembedded EG. Furthermore, the low ligand density disc expands the Rg of EG chains more than other discs.

As it was explained for the shell entropy loss, high ligand density disc with a rapid penetration rate encounters the higher surface tension of EG at the water/EG interface. As a result, the penetration of the high ligand density disc leads to higher EG entropy loss and a lower Rg of EG chains.

On the other hand, ligand entropy loss (Figure 6k) is lower for NCs with the higher ligand densitiy.. In fact, the high ligand density NC has more ligands at the interface of EG/water with a very attractive interaction to the EG layer. This highly attractive interaction and increase in the Rg of EG chains offers the ligand chains more freedom to move. Therefore at this ligand density, the NC has more disordered ligand chains. Overall, the ligand entropy is a weak barrier for the pentertaion of high ligand density NCs.

Furthermore, the disc with 340 ligands, with more ordered EG chains produces a more entropy loss of the receptors (Figures 6l and S16) than the disc with 170 ligands ergo the receptor entropy loss is a barrier for the penetration of the high ligand density disc.

Using a Monte Carlo simulation Liu et al.[36] found that the targeting of NCs to endothelial cells enhances by the increase in ligand density of NCs.

In our work also, the disc with 340 ligands presents more barriers for penetration, including high shell entropy loss. However, its substantial driving forces from low potential energy and receptor entropy loss can overcome these barriers, leading to its exceptionally fast dynamics.

Indeed for each individual property of a NC the peneteration depth is governed by the interplay of energies and entropies generated by that specific property.

In contrast, for each NC with a combination of properties, the penetration depth is determined by the complex interplay of all energies and entropies that are induced by that specific combination of properties.

Subsequently, there is not a direct relation between the penetration depth of a NC and each property of that NCs.

To put in another way it is not possible to claim that always a specific property provokes or prevents NCs penetration.

For instance the disc shape and the 12 R_c NC with the high ligand density can penetrate deeper inside the EG layer than other shapes and sizes, respectively. Conversely, the sphere shape or 16 R_c NCs at their high ligand density, have lower penetration depth or slower penetration speed than others shapes or smallers sizes, respectively.

Moreover, the negatively charged nature of EG chains provides a charge barrier for blood vessels[80]. In fact, EG chains can adhere to plasma proteins and ions with positive charges. Therefore, it is important to study the effect of charged EG on adhesion and penetration of charged NCs.

There are also studies about ion molecules and charged colloids in contact with charged surfaces and mixed fluid vesicles[81,82].

Therefore, the influence of adding positive charge to NCs on the penetration depth of NCs and the free energy perturbation in the drug delivery system are also worth exploring.

4. Conclusion and summary

We have studied the adhesion and penetration process of nanocarriers (NCs) with different surface chemistry of varying shapes, sizes, and initial orientations to endothelial cells. The mechanism of potential energy gains and entropy losses in a series of parameters, such as EG, ligands, NC shell, and receptors were systemically investigated.

The shape effect expressed that although initially spheres and rods have higher driving forces than discs due to the larger local surface area at the EG/water interface, barriers such as the shell entropy loss for the former is larger, therefore discs show the best penetration amount. In fact, the NC shape with the weaker mechanical stiffness has more barriers to penetration. In other words, at a specific driving force for different shapes of NCs, the shell entropy loss controls the penetration of NCs. Moreover, the rotation of the disc during penetration is an extra driving force.

Size effects imply that at a specific ligand density, there is a threshold for the NC size. For a NC with larger size than the threshold size, the driving force cannot overcome barriers such as the shell entropy loss. Therefore, for larger NCs, it is necessary to either increase the ligand density or improve the mechanical stiffness of the NC. In other words, at a specific ligand density by tuning the size and stiffness of the NCs, the barriers can be diminished and therefore enhance the adsorption of NCs to the cell.

The initial orientation effect demonstrates that the best orientation for the penetration of the disc NC is the perpendicular one. On the other hand, perpendicular orientation has higher potential energy and thus is less favorable than parallel orientation. Moreover, the perpendicular orientation of the disc NC has more entropy losses of the shell and ligand chains. Nevertheless, it can exceed the lower driving force and higher barriers with the help of rotating clockwise and counterclockwise, and this feature has a stronger effect on the penetration than the shell and ligands entropy loss.

In what concerns the ligand density effect, although the NC with higher ligand density has more shell entropy loss, its lower ligand entropy loss and the favorable energetic behavior leads to faster dynamics. In fact, an increase in the ligand density results in an increase in the driving force and in barriers. Consequently, for each NC, a proper ligand density is required so that driving forces can overcome barriers.

In conclusion, for the initial orientation, shape, and size effects on the NC penetration, the NC shell entropy is a dominant factor. Besides, when the NC is at the EG/water interface, the NC feels the whole surface tension of the EG layer only on the surface area of its edge. Though, when the NC is inside the EG layer, the whole volume of the NC feels the osmotic pressure of EG chains.

5. Conflict of interest

There are no conflicts to declare.

6. Acknowledgments

This work was supported by the NSF grant CBET 1703919.

7. References:

(1) Sabri, S. Glycocalyx Modulation Is a Physiological Means of Regulating Cell Adhesion. **2000**.

(2) Agrawal, N. J.; Radhakrishnan, R. The Role of Glycocalyx in Nanocarrier-Cell Adhesion Investigated Using a Thermodynamic Model and Monte Carlo Simulations †. https://doi.org/10.1021/jp074514x.

(3) Sakhalkar, H. S.; Dalal, M. K.; Salem, A. K.; Ansari, R.; Fu, J.; Kiani, M. F.; Kurjiaka, D. T.; Hanes, J.; Shakesheff, K. M.; Goetz, D. J. Leukocyte-Inspired Biodegradable Particles That Selectively and Avidly Adhere to Inflamed Endothelium in Vitro and in Vivo. *Proc. Natl. Acad. Sci. U. S. A.* **2003**, *100* (26), 15895–15900. https://doi.org/10.1073/pnas.2631433100.

(4) Farokhirad, S.; Ranganathan, A.; Myerson, J.; Muzykantov, V. R.; Ayyaswamy, P. S.; Eckmann, D. M.; Radhakrishnan, R. Stiffness Can Mediate Balance between Hydrodynamic Forces and Avidity to Impact the Targeting of Flexible Polymeric Nanoparticles in Flow. *Nanoscale* **2019**, *11* (14), 6916–6928. https://doi.org/10.1039/c8nr09594a.

(5) Mulivor, A. W.; Lipowsky, H. H. Role of Glycocalyx in Leukocyte-Endothelial Cell Adhesion. *Am. J. Physiol. - Hear. Circ. Physiol.* **2002**, *283* (4 52-4), 1282–1291. https://doi.org/10.1152/ajpheart.00117.2002.

(6) Muro, S.; Garnacho, C.; Champion, J. A.; Leferovich, J.; Gajewski, C.; Schuchman, E. H.; Mitragotri, S.; Muzykantov, V. R. Control of Endothelial Targeting and Intracellular Delivery of Therapeutic Enzymes by Modulating the Size and Shape of ICAM-1-Targeted Carriers. *Mol. Ther.* **2008**, *16* (8), 1450–1458. https://doi.org/10.1038/mt.2008.127.

(7) Elias, D. R.; Poloukhtine, A.; Popik, V.; Tsourkas, A. Effect of Ligand Density, Receptor Density, and Nanoparticle Size on Cell Targeting. *Nanomedicine Nanotechnology, Biol. Med.* **2013**, *9* (2), 194–201. https://doi.org/10.1016/J.NANO.2012.05.015.

(8) Decuzzi, P.; Godin, B.; Tanaka, T.; Lee, S. Y.; Chiappini, C.; Liu, X.; Ferrari, M. Size and Shape Effects in the Biodistribution of Intravascularly Injected Particles. *J. Control. Release* **2010**, *141* (3), 320–327. https://doi.org/10.1016/J.JCONREL.2009.10.014.

(9) Blanco, E.; Shen, H.; Ferrari, M. Principles of Nanoparticle Design for Overcoming Biological Barriers to Drug Delivery. **2015**. https://doi.org/10.1038/nbt.3330.

(10) Moghimi, S. M.; Hunter, A. C.; Andresen, T. L. Downloaded from Www.Annualreviews.Org Access Provided by Case Western Reserve-Kelvin Smith Library on 08/18/21. For Personal Use Only. *Annu. Rev. Pharmacol. Toxicol* **2012**, *52*, 481–503. https://doi.org/10.1146/annurev-pharmtox-010611-134623.

(11) Nel, A. E.; Mädler, L.; Velegol, D.; Xia, T.; V Hoek, E. M.; Somasundaran, P.; Klaessig, F.; Castranova, V.; Thompson, M. Understanding Biophysicochemical Interactions at the Nano–Bio Interface. *Nat. Publ. Gr.* **2009**. https://doi.org/10.1038/nmat2442.

(12) Shang, L.; Nienhaus, K.; Nienhaus, G. U. Engineered Nanoparticles Interacting with Cells: Size Matters. *Journal of Nanobiotechnology*. BioMed Central February 3, 2014, pp 1–11. https://doi.org/10.1186/1477-3155-12-5.

(13) Muro, S.; Dziubla, T.; Qiu, W.; Leferovich, J.; Cui, X.; Berk, E.; Muzykantov, V. R. Endothelial Targeting of High-Affinity Multivalent Polymer Nanocarriers Directed to Intercellular Adhesion Molecule 1. *J. Pharmacol. Exp. Ther.* **2006**, *317* (3), 1161–1169. https://doi.org/10.1124/jpet.105.098970.

(14) Haun, J. B.; Hammer, D. A. Quantifying Nanoparticle Adhesion Mediated by Specific Molecular Interactions. *Langmuir* **2008**, *24* (16), 8821–8832. https://doi.org/10.1021/la8005844.

(15) McKenzie, M.; Ha, S. M.; Rammohan, A.; Radhakrishnan, R.; Ramakrishnan, N. Multivalent Binding of a Ligand-Coated Particle: Role of Shape, Size, and Ligand Heterogeneity. *Biophys. J.* **2018**, *114* (8), 1830–1846. https://doi.org/10.1016/j.bpj.2018.03.007.

(16) Shukla, S.; Eber, F. J.; Nagarajan, A. S.; Difranco, N. A.; Schmidt, N.; Wen, A. M.; Eiben, S.; Twyman, R. M.; Wege, C.; Steinmetz, N. F. The Impact of Aspect Ratio on the Biodistribution and Tumor Homing of Rigid Soft-Matter Nanorods. *Adv. Healthc. Mater.* **2015**, *4* (6), 874–882. https://doi.org/10.1002/adhm.201400641.

(17) Wen, A. M.; Pooja, ·; Rambhia, H.; French, R. H.; Steinmetz, N. F.; Wen, A. M.; Steinmetz, N. F.; Rambhia, P. H.; French, R. H.; Steinmetz, · N F. Design Rules for Nanomedical Engineering: From Physical Virology to the Applications of Virus-Based Materials in Medicine. *J Biol Phys* **2013**, *39*, 301–325. https://doi.org/10.1007/s10867-013-9314-z.

(18) Champion, J. A.; Mitragotri, S. Role of Target Geometry in Phagocytosis. **2006**.

(19) Kim, J. U.; O'Shaughnessy, B. Nanoinclusions in Dry Polymer Brushes. *Macromolecules* **2006**, *39* (1), 413–425. https://doi.org/10.1021/ma050817i.

(20) Daddi-Moussa-Ider, A.; Goh, S.; Liebchen, B.; Hoell, C.; Mathijssen, A. J. T. M.; Guzmán-Lastra, F.; Scholz, C.; Menzel, A. M.; Löwen, H. Membrane Penetration and Trapping of an Active Particle. *J. Chem. Phys.* **2019**, *150* (6). https://doi.org/10.1063/1.5080807.

(21) Romeis, D.; Sommer, J. U. Conformational Switching of Modified Guest Chains in Polymer Brushes. *J. Chem. Phys.* **2013**, *139* (4), 044910. https://doi.org/10.1063/1.4816125.

(22) Vogiatzis, G. G.; Theodorou, D. N. Structure of Polymer Layers Grafted to Nanoparticles in Silica-Polystyrene Nanocomposites. *Macromolecules* **2013**, *46* (11), 4670–4683. https://doi.org/10.1021/ma400107q.

(23) Zhang, Q.; Xiang, X. Adsorption of a Spherical Nanoparticle in Polymer Brushes: Brownian Dynamics Investigation. *Phys. A Stat. Mech. its Appl.* **2013**, *392* (18), 3857–3862. https://doi.org/10.1016/j.physa.2013.05.001.

(24) Guskova, O. A.; Pal, S.; Seidel, C. Organization of Nanoparticles at the Polymer Brush-Solvent Interface. *Europhys. Lett.* **2009**, *88* (3), 38006. https://doi.org/10.1209/0295-5075/88/38006.
(25) Kim, J. U.; Matsen, M. W. Repulsion Exerted on a Spherical Particle by a Polymer Brush. *Macromolecules* **2008**, *41* (1), 246–252. https://doi.org/10.1021/ma071906t.
(26) Halperin, A.; Kr€, M.; Zhulina, E. B. Colloid-Brush Interactions: The Effect of Solvent Quality. **2011**, *44*, 3622–3638. https://doi.org/10.1021/ma200068d.
(27) Lewis, T.; Ganesan, V. Interactions between Grafted Cationic Dendrimers and Anionic Bilayer Membranes. *J. Phys. Chem. B* **2013**, *117* (33), 9806–9820. https://doi.org/10.1021/jp4053049.
(28) Surve, M.; Pryamitsyn, V.; Ganesan, V. Polymer-Bridged Gels of Nanoparticles in Solutions of Adsorbing Polymers. *J. Chem. Phys.* **2006**, *125* (6), 064903. https://doi.org/10.1063/1.2241150.
(29) Chen, K.; Ma, Y. Q. Interactions between Colloidal Particles Induced by Polymer Brushes Grafted onto the Substrate. *J. Phys. Chem. B* **2005**, *109* (37), 17617–17622. https://doi.org/10.1021/jp051403u.
(30) Egorov, S. A.; Binder, K. Effect of Solvent Quality on the Dispersibility of Polymer-Grafted Spherical Nanoparticles in Polymer Solutions. *J. Chem. Phys.* **2012**, *137* (9), 094901. https://doi.org/10.1063/1.4747196.
(31) Merlitz, H.; Wu, C. X.; Sommer, J. U. Inclusion Free Energy of Nanoparticles in Polymer Brushes. *Macromolecules* **2012**, *45* (20), 8494–8501. https://doi.org/10.1021/ma301781b.
(32) Curk, T.; Martinez-Veracoechea, F. J.; Frenkel, D.; Dobnikar, J. Collective Ordering of Colloids in Grafted Polymer Layers. *Soft Matter* **2013**, *9* (23), 5565–5571. https://doi.org/10.1039/c3sm50486g.
(33) Chen, B.; Fu, B. M. An Electrodiffusion-Filtration Model for Effects of Endothelial Surface Glycocalyx on Microvessel Permeability to Macromolecules. *J. Biomech. Eng.* **2004**, *126* (5), 614–624. https://doi.org/10.1115/1.1800571.
(34) Weinbaum, S.; Zhang, X.; Han, Y.; Vink, H.; Cowin, S. C. Mechanotransduction and Flow across the Endothelial Glycocalyx. *Proc. Natl. Acad. Sci. U. S. A.* **2003**, *100* (13), 7988–7995. https://doi.org/10.1073/pnas.1332808100.
(35) Liu, J.; Ayyaswamy, P. S.; Eckmann, D. M.; Radhakrishnan, R. Modelling of Binding Free Energy of Targeted Nanocarriers to Cell Surface. *Heat Mass Transf. und Stoffuebertragung* **2014**, *50* (3), 315–321. https://doi.org/10.1007/s00231-013-1274-0.
(36) Liu, J.; Weller, G. E. R.; Zern, B.; Ayyaswamy, P. S.; Eckmann, D. M.; Muzykantov, V. R.; Radhakrishnan, R. Computational Model for Nanocarrier Binding to Endothelium Validated Using in Vivo, in Vitro, and Atomic Force Microscopy Experiments. *Proc. Natl. Acad. Sci. U. S. A.* **2010**, *107* (38), 16530–16535. https://doi.org/10.1073/pnas.1006611107.
(37) Farokhirad, S.; Bradley, R. P.; Radhakrishnan, R. Thermodynamic Analysis of Multivalent Binding of Functionalized Nanoparticles to Membrane Surface Reveals the Importance of Membrane Entropy and Nanoparticle Entropy in Adhesion of Flexible Nanoparticles. *Soft Matter* **2019**, *15* (45), 9271–9286. https://doi.org/10.1039/c9sm01653h.
(38) Kabedev, A.; Lobaskin, V. Structure and Elasticity of Bush and Brush-like Models of the Endothelial Glycocalyx. *Sci. Rep.* **2018**, *8* (1), 240. https://doi.org/10.1038/s41598-017-18577-3.

(39) Li, Y.; Yue, T.; Yang, K.; Zhang, X. Molecular Modeling of the Relationship between Nanoparticle Shape Anisotropy and Endocytosis Kinetics. *Biomaterials* **2012**, *33* (19), 4965–4973. https://doi.org/10.1016/J.BIOMATERIALS.2012.03.044.
(40) Li, Y.; Niu, X.; Li, L.; Zhang, X.; Yang, K.; Yue, T. Size, Geometry and Mobility of Protein Assemblage Regulate the Kinetics of Membrane Wrapping on Nanoparticles. *Journal of Molecular Liquids*. 2021. https://doi.org/10.1016/j.molliq.2021.115990.
(41) Li, Y.; Zhang, M.; Niu, X.; Yue, T. Selective Membrane Wrapping on Differently Sized Nanoparticles Regulated by Clathrin Assembly: A Computational Model. *Colloids and Surfaces B: Biointerfaces*. 2022, p 112467. https://doi.org/10.1016/j.colsurfb.2022.112467.
(42) Cruz-Chu, E. R.; Malafeev, A.; Pajarskas, T.; Pivkin, I. V.; Koumoutsakos, P. Structure and Response to Flow of the Glycocalyx Layer. *Biophys. J.* **2014**, *106* (1), 232–243. https://doi.org/10.1016/j.bpj.2013.09.060.
(43) Zhang, X.; Adamson, R. H.; Curry, F.-R. E.; Weinbaum, S. A 1-D Model to Explore the Effects of Tissue Loading and Tissue Concentration Gradients in the Revised Starling Principle. *Am. J. Physiol. Circ. Physiol.* **2006**, *291* (6), H2950–H2964. https://doi.org/10.1152/ajpheart.01160.2005.
(44) Deng, M.; Li, X.; Liang, H.; Caswell, B.; Karniadakis, G. E. Simulation and Modelling of Slip Flow over Surfaces Grafted with Polymer Brushes and Glycocalyx Fibres. *J. Fluid Mech.* **2012**, *711*, 192–211. https://doi.org/10.1017/jfm.2012.387.
(45) Li, Y.; Kröger, M.; Liu, W. K. Shape Effect in Cellular Uptake of PEGylated Nanoparticles: Comparison between Sphere, Rod, Cube and Disk. *Nanoscale* **2015**, *7* (40), 16631–16646. https://doi.org/10.1039/c5nr02970h.
(46) Yang, K.; Ma, Y. Q. Computer Simulation of the Translocation of Nanoparticles with Different Shapes across a Lipid Bilayer. *Nat. Nanotechnol.* **2010**, *5* (8), 579–583. https://doi.org/10.1038/nnano.2010.141.
(47) Paiva, F. L.; Secchi, A. R.; Calado, V.; Maia, J.; Khani, S. Slip and Momentum Transfer Mechanisms Mediated by Janus Rods at Polymer Interfaces. *Soft Matter* **2020**, *16* (28), 6662–6672. https://doi.org/10.1039/d0sm00858c.
(48) Jamali, S.; Yamanoi, M.; Maia, J. Bridging the Gap between Microstructure and Macroscopic Behavior of Monodisperse and Bimodal Colloidal Suspensions. *Soft Matter* **2013**, *9* (5), 1506–1515. https://doi.org/10.1039/c2sm27104d.
(49) Khani, S.; Jamali, S.; Boromand, A.; Hore, M. J. A.; Maia, J. Polymer-Mediated Nanorod Self-Assembly Predicted by Dissipative Particle Dynamics Simulations. *Soft Matter*. 2015, pp 6881–6892. https://doi.org/10.1039/c5sm01560j.
(50) Boromand, A.; Jamali, S.; Maia, J. M. Structural Fingerprints of Yielding Mechanisms in Attractive Colloidal Gels. *Soft Matter*. 2017, pp 458–473. https://doi.org/10.1039/C6SM00750C.
(51) Barcelos, E. I.; Khani, S.; Boromand, A.; Vieira, L. F.; Lee, A. J.; Peet, J.; Naccache, M.; Maia, J. *Controlling Particle Penetration and Depletion at the Wall Using Dissipative Particle Dynamics*; 2020.
(52) Kobayashi, Y.; Arai, N. Janus or Homogeneous Nanoparticle Mediated Self-Assembly of Polymer Electrolyte Fuel Cell Membranes. *RSC Adv.* **2018**, *8* (33), 18568–18575. https://doi.org/10.1039/c8ra03187h.
(53) Jehser, M.; Zifferer, G.; Likos, C. N. Scaling and Interactions of Linear and Ring Polymer Brushes via DPD Simulations. *Polymers (Basel).* **2019**, *11* (3).

https://doi.org/10.3390/polym11030541.
(54) Wang, Y.; Li, Z.; Xu, J.; Yang, C.; Karniadakis, G. E. Concurrent Coupling of Atomistic Simulation and Mesoscopic Hydrodynamics for Flows over Soft Multi-Functional Surfaces. *Soft Matter* **2019**, *15* (8), 1747–1757. https://doi.org/10.1039/c8sm02170h.
(55) Li, Z.; Bian, X.; Tang, Y. H.; Karniadakis, G. E. A Dissipative Particle Dynamics Method for Arbitrarily Complex Geometries. *J. Comput. Phys.* **2018**, *355*, 534–547. https://doi.org/10.1016/j.jcp.2017.11.014.
(56) Jaime A. Millan, Wenhua Jiang, M. L. Pressure Driven Flow of Polymer Solutions in Nanoscale Slit Pores Pressure Driven Flow of Polymer Solutions in Nanoscale Slit Pores. **2007**, *124905* (January 2007). https://doi.org/10.1063/1.2711435.
(57) Cheng, J.; Vishnyakov, A.; Neimark, A. V. Adhesion of Nanoparticles to Polymer Brushes Studied with the Ghost Tweezers Method. *J. Chem. Phys.* **2015**, *142* (3), 034705. https://doi.org/10.1063/1.4905894.
(58) Biagi, S.; Rovigatti, L.; Sciortino, F.; Misbah, C. Surface Wave Excitations and Backflow Effect over Dense Polymer Brushes OPEN. **2016**. https://doi.org/10.1038/srep22257.
(59) Santo, K. P.; Vishnyakov, A.; Brun, Y.; Neimark, A. V. Critical Conditions of Adhesion and Separation of Functionalized Nanoparticles on Polymer Grafted Substrates. *J. Phys. Chem. C* **2019**, *123* (26), 16091–16106. https://doi.org/10.1021/acs.jpcc.9b01219.
(60) Groot, R. D.; Warren, P. B. Dissipative Particle Dynamics: Bridging the Gap between Atomistic and Mesoscopic Simulation. *J. Chem. Phys.* **1997**, *107* (11), 4423–4435. https://doi.org/10.1063/1.474784.
(61) Cho, E. C.; Au, L.; Zhang, Q.; Xia, Y. The Effects of Size, Shape, and Surface Functional Group of Gold Nanostructures on Their Adsorption and Internalization by Cells. *Small* **2010**, *6* (4), 517–522. https://doi.org/10.1002/SMLL.200901622.
(62) Chen, H.; Paholak, H.; Ito, M.; Sansanaphongpricha, K.; Qian, W.; Che, Y.; Sun, D. "Living" PEGylation on Gold Nanoparticles to Optimize Cancer Cell Uptake by Controlling Targeting Ligand and Charge Densities. *IOP Publ. Nanotechnol. Nanotechnol.* **2013**, *24*, 355101–355110. https://doi.org/10.1088/0957-4484/24/35/355101.
(63) Amini, M.; Hasheminejad, K.; Montazeri, A. Experimentally Guided MD Simulation to Enhance the Shape Memory Behavior of Polymer-Based Nanocomposites: Towards Elaborating the Underlying Mechanism. *Compos. Part A Appl. Sci. Manuf.* **2020**, *138*, 106055. https://doi.org/10.1016/j.compositesa.2020.106055.
(64) Gong, Y.; Ma, X.; Luo, K. H.; Xu, H.; Shuai, S. A Molecular Dynamics Study of Evaporation Mode Transition of Hydrocarbon Fuels under Supercritical Conditions. *Combust. Flame* **2022**, *246*, 112397. https://doi.org/10.1016/J.COMBUSTFLAME.2022.112397.
(65) Ghaffarizadeh, S. A.; Wang, G. J. Excess Entropy Scaling in Active-Matter Systems. *Journal of Physical Chemistry Letters*. 2022, pp 4949–4954. https://doi.org/10.1021/acs.jpclett.2c01415.
(66) Champion, J. A.; Katare, Y. K.; Mitragotri, S. Particle Shape: A New Design Parameter for Micro-and Nanoscale Drug Delivery Carriers. **2007**. https://doi.org/10.1016/j.jconrel.2007.03.022.
(67) Le, T. C.; Zhai, J.; Chiu, W.-H.; Tran, P. A.; Tran, N. Janus Particles: Recent Advances in the Biomedical Applications. **2019**. https://doi.org/10.2147/IJN.S169030.
(68) Li, C.-W.; Merlitz, H.; Wu, C.-X.; Sommer, J.-U. Nanopores as Switchable Gates for

Nanoparticles: A Molecular Dynamics Study. **2018**. https://doi.org/10.1021/acs.macromol.8b01149.

(69) Leónforte, F.; Mü, M. Functional Poly(N-Isopropylacrylamide)/Poly(Acrylic Acid) Mixed Brushes for Controlled Manipulation of Nanoparticles. **2016**. https://doi.org/10.1021/acs.macromol.6b00535.

(70) Agrawal, G.; Agrawal, R. Janus Nanoparticles: Recent Advances in Their Interfacial and Biomedical Applications. **2019**. https://doi.org/10.1021/acsanm.9b00283.

(71) Gao, H. M.; Li, B.; Zhang, R.; Sun, Z. Y.; Lu, Z. Y. Free Energy for Inclusion of Nanoparticles in Solvated Polymer Brushes from Molecular Dynamics Simulations. *J. Chem. Phys.* **2020**, *152* (9), 094905. https://doi.org/10.1063/5.0002257.

(72) Ding, H. M.; Ma, Y. Q. Theoretical and Computational Investigations of Nanoparticle-Biomembrane Interactions in Cellular Delivery. *Small*. Wiley-VCH Verlag March 11, 2015, pp 1055–1071. https://doi.org/10.1002/smll.201401943.

(73) Yi, X.; Shi, X.; Gao, H. Cellular Uptake of Elastic Nanoparticles. **2011**, *87*. https://doi.org/10.1103/PhysRevLett.107.098101.

(74) Yue, T.; Zhang, X. Molecular Modeling of the Pathways of Vesicle-Membrane Interaction †. https://doi.org/10.1039/c2sm26940f.

(75) Sadhu, R. K.; Barger, S. R.; Penič, S.; Iglič, A.; Krendel, M.; Gauthier, N. C.; Gov, N. S. A Theoretical Model of Efficient Phagocytosis Driven by Curved Membrane Proteins and Active Cytoskeleton Forces. *Soft Matter* **2022**, *19* (1), 31–43. https://doi.org/10.1039/D2SM01152B.

(76) Sharma, G.; Sharma, A. R.; Lee, S. S.; Bhattacharya, M.; Nam, J. S.; Chakraborty, C. Advances in Nanocarriers Enabled Brain Targeted Drug Delivery across Blood Brain Barrier. *International Journal of Pharmaceutics*. Elsevier B.V. March 25, 2019, pp 360–372. https://doi.org/10.1016/j.ijpharm.2019.01.056.

(77) Yang, K.; Ma, Y.-Q. Computer Simulation of the Translocation of Nanoparticles with Different Shapes across a Lipid Bilayer. *Nat. Nanotechnol.* | **2010**, *5*. https://doi.org/10.1038/NNANO.2010.141.

(78) Wang, D.; Nap, R. J.; Lagzi, I.; Kowalczyk, B.; Han, S.; Grzybowski, B. A.; Szleifer, I. How and Why Nanoparticle's Curvature Regulates the Apparent PKa of the Coating Ligands. *J. Am. Chem. Soc.* **2011**, *133* (7), 2192–2197. https://doi.org/10.1021/JA108154A.

(79) Walker, D. A.; Leitsch, E. K.; Nap, R. J.; Szleifer, I.; Grzybowski, B. A. Geometric Curvature Controls the Chemical Patchiness and Self-Assembly of Nanoparticles. *Nat. Nanotechnol. 2013 89* **2013**, *8* (9), 676–681. https://doi.org/10.1038/nnano.2013.158.

(80) Jin, J.; Fang, F.; Gao, W.; Chen, H.; Wen, J.; Wen, X.; Chen, J. The Structure and Function of the Glycocalyx and Its Connection With Blood-Brain Barrier. *Front. Cell. Neurosci.* **2021**, *15*. https://doi.org/10.3389/FNCEL.2021.739699.

(81) Gongadze, E.; Velikonja, A.; Perutkova, S.; Kramar, P.; Maček-Lebar, A.; Kralj-Iglič, V.; Iglič, A. Ions and Water Molecules in an Electrolyte Solution in Contact with Charged and Dipolar Surfaces. *Electrochim. Acta* **2014**, *126*, 42–60. https://doi.org/10.1016/j.electacta.2013.07.147.

(82) Fošnarič, M.; Iglič, A.; Kroll, D. M.; May, S. Monte Carlo Simulations of Complex Formation between a Mixed Fluid Vesicle and a Charged Colloid. *J. Chem. Phys.* **2009**, *131* (10), 105103. https://doi.org/10.1063/1.3191782/906269.